ORIGINAL ARTICLE

Evaluation of the Usefulness of the Myocardial Flow Reserve Index Using an Anger-Type SPECT/CT System

Atsushi Komuro[1)], Rika Endo[1)], Mika Tanno[1)], Kouichi Ishimori[1)], Kazuo Funaki[1)], Jiro Izumida, MD[2)], and Tomiyoshi Saito, MD[2)]

Received: August 9, 2024 / Revised manuscript received: January 6, 2025 / Accepted: January 8, 2025
J-STAGE advance published: February 14, 2025

Abstract

***Background*: The quantitative analysis of myocardial blood flow and myocardial flow reserve (MFR) is expected to address challenges in evaluating the relative distribution of myocardial perfusion imaging. This study aimed to determine the normal range of MFR index using the myocardial uptake ratio (MUR) method in normal volunteers (NV) with an Anger-type single photon emission computed tomography/computed tomography (SPECT/CT) system and to evaluate its diagnostic accuracy for ischemic heart disease (IHD) and heart failure (HF).**

***Method*: Two methods for calculating the MUR were evaluated. The area under the curve (AUC) method utilized the AUC of the time-activity curve (TAC) of the aortic arch as the input function (AUC-based MFR index). The DOSE method employed the dose activity (dose-based MFR index). IHD was categorized into single-vessel disease (SVD) and multivessel disease (MVD; double- and triple-vessel disease combined).**

***Results*: Normal range of AUC-based MFR index was 1.63 ± 0.30, 1.40 ± 0.24 for SVD, 1.28 ± 0.17 for MVD, and 1.11 ± 0.12 for HF. The normal range of the dose-based MFR index was 1.18 ± 0.14, 1.15 ± 0.26 for SVD, 1.02 ± 0.10 for MVD, and 0.99 ± 0.06 for HF. Significant differences were observed among the NV, MVD, and HF groups. No significant differences were noted between NV and SVD groups. The results of the receiver operating characteristic curve (ROC) analysis in combination with NV showed that the AUC of the ROC curve was 0.732 (95%CI 0.542–0.922) for SVD, 0.841 (95%CI 0.717–0.965) for MVD, and 0.969 (95%CI, 0. 922–1.0) for HF. The AUC of dose-based MFR index were 0.667 (95%CI 0.404–0.929) for SVD, 0.817 (95%CI 0.684–0.950) for MVD, and 0.908 (95%CI 0.814–1.0) for HF. DeLong's test showed no significant differences between the AUC of AUC-based and dose-based MFR indices.**

***Conclusion*: The findings suggest the potential clinical application of AUC and DOSE methods for quantitative analysis of the MFR index using an Anger-type SPECT/CT system. These methods are expected to enhance the accuracy of diagnosis and prognosis in patients with IHD and HF.**

Keywords: Anger-type single photon emission computed tomography, Area under the curve (AUC), Myocardial flow reserve index (MFR index), Myocardial uptake ratio (MUR)
Ann Nucl Cardiol 2025; 11 (1): 13–19

The utility of electrocardiogram (ECG)-gated single-photon emission computed tomography (SPECT) myocardial perfusion imaging (MPI) for detecting left main stem and three-vessel coronary artery disease remains underexplored (1, 2). These patients are at a higher risk of adverse cardiac events and may benefit significantly from revascularization (3, 4).

Quantitative analysis of myocardial blood flow (MBF) and myocardial flow reserve (MFR) offers a potential solution to address challenges in evaluating relative blood flow distribution in MPI. Traditionally, MBF quantification at stress and rest (ml/g/min) and the determination of MFR have been the

DOI: 10.17996/anc.24-00005

1) Department of Radiology, Shirakawa Kosei General Hospital, Fukushima, Japan
2) Department of Cardiovascular Internal Medicine, Shirakawa Kosei General Hospital, Fukushima, Japan

domains of positron emission tomography (PET) MPI using tracers such as ^{15}O-water, $^{13}NH_3$-ammonia, and ^{82}Rubidium (5). The additional prognostic value of MFR measurements, beyond standard ischemia assessments, was conclusively demonstrated in two large studies (6, 7). Furthermore, flow measurements have shown potential diagnostic value for better prediction of obstructive coronary disease (8, 9). Revascularization-targeting regions with reduced coronary flow capacity and relative perfusion abnormalities on baseline PET showed significant improvements in stress MBF. When revascularization was performed in regions without reduced coronary flow capacity, the stress MBF did not improve (10). Patients with ischemic heart disease (IHD) revascularized based on PET viability assessments and reduced MFR are at an increased risk of cardiac death and subsequent cardiac events. Notably, MFR is a more sensitive predictor of cardiac death compared to left ventricular ejection fraction or extent of viability (11).

Recent advancements in cardiac-dedicated SPECT systems with dynamic SPECT have driven efforts to develop and validate SPECT MBF protocols (10, 11).

While PET offers well-validated and easily obtainable blood flow measurements, SPECT remains a more widely used MPI technique globally. Evaluation methods for the MFR index using standard SPECT equipment have been reported previously (12–21). These methods apply the myocardial uptake ratio (MUR) based on either the area under the curve (AUC) of the time-activity curve (TAC) from the aortic arch or pulmonary artery (12–19) (AUC method), or the injection dose (20, 21) (DOSE method).

This study aimed to establish the normal range for the MFR index (AUC-based and dose-based MFR index) in normal volunteers (NV) and evaluate the diagnostic accuracy of these methods for IHD and heart failure (HF) using receiver operating characteristic curve (ROC) analysis in combination with NV.

Materials and methods

Algorithm for AUC method and DOSE method (21)

If the intramyocardial behavior of ^{99m}Tc-methoxyisobutylisonitrile (^{99m}Tc-MIBI) resembles that of chemical microspheres, MBF can be determined using the myocardial tissue radioactivity Cmc(T) (Bq/g) obtained via myocardial SPECT at time T after ^{99m}Tc-MIBI administration and the input function Ca(t) (Bq/mL) of arterial blood. The MBF mL/g/min was calculated using the following equation:

$$MBF=Cmc(T)\ /\int_o^t Ca(t)dt$$

In the AUC method, the AUC approximates the first circulating component of the TAC of the aorta using the gamma function as a correlated parameter derived from in vitro measurements without arterial blood sampling. The MUR was proportional to MBF and was defined using the following equation:

$$MUR=Cmc(T)/AUC\times 100$$

Cmc(T) in this method was obtained as a SPECT count, whereas the AUC was a planar count, leading to geometric discrepancies. A cross-calibration factor (SPECT-planar cross calibration factor[CCF], CCF[SP]) was used to address this discrepancy.

$$MUR=Cmc(T)\times CCF(SP)/AUC\times 100$$

The same region of interest (ROI) was outlined on the myocardium of the acquired image of the anterior view of the resting SPECT acquisition image and the planar image of the same view before second ^{99m}Tc-MIBI loading. The effective half-life (eHL) was calculated from the average counts of the heart ROI for each image (RestH, RestResidualH) and the acquisition time difference (t) using the following equation:

$$eHL=-t/(log_2[RestResidualH/RestH])$$

The residual first scan count during the second scan was calculated and subtracted using eHL. The MUR at rest and stress were defined as rest MUR and stress MUR, respectively. The AUC-based MFR index was calculated using the following equation:

$$AUC\text{-}based\ MFR\ index=stress\ MUR/rest\ MUR$$

In the DOSE method, the residual first scan count in the second scan is calculated and subtracted using the physical half-life of ^{99m}Tc to increase versatility. The dose-based MFR index was calculated from the Cmc(T) of the subtracted stress and rest (StrC, RstC) and the injected dose [MBq] of stress and rest (StrD, RstD) at stress and rest using the following equation:

$$dose\text{-}based\ MFR\ index=\frac{StrC}{StrD}/\frac{RstC}{RstD}$$

Equipment

A Symbia T6 SPECT/CT system (Siemens Healthineers, Erlangen, Germany) equipped with a low-energy, high-resolution (LEHR) collimator was used for image acquisition. Image processing was conducted on an image processing workstation (Syngo MI Apps; Siemens Healthineers). The autoinjector used was an AutoEnhance A-60 (Nemoto Kyorindo, Tokyo, Japan) and the dose calibrator (Curiemeter

Table 1

Acquisition		
Collimator		LEHR
Matrix size		128×128
Pixel size		3.3 mm
Number of view		60 views/360 degree
Time per view	Rest	about 50 sec*
	Stress	about 20 sec*
Frame per cycle		16

Reconstruction	
Method	OSEM
	Iteration：12
	Subset：6
Smoothing filter	Gaussian
	FWHM：13.2 mm
Attenuation correction	X-CT
Scatter correction	DEW
Resolution recovery	+

* Time was set when the average count of the myocardium in the anterior view reached 30 counts/pixel

IGC-7; Aloka, Tokyo, Japan).

The QGS/QPS software (version 2012; Cedars Sinai Medical Center, California, USA) was utilized to calculate ejection fraction and defect scores. For quantitative analysis of myocardial blood flow, CardioBULL and MIBI MFR software (PDRadiopharma, Tokyo, Japan) running on a Windows PC were used. Microsoft Excel 365 and EZR (22) were used for graphing and statistical analyses.

CCF measurement

A syringe containing ^{99m}Tc (16.2 MBq and 1.0 mL was placed 30 cm parallel to the detector, and the total count in the field of view was recorded under the same conditions as the clinical dynamic acquisition. The solution was subsequently diluted and transferred into a cylindrical phantom (3,016 mL), and imaging was performed under identical clinical SPECT conditions. The ROI was set on the reconstructed images and the average value was calculated.

The planar counts (counts/min), phantom volume (V, mL), and average values of the SPECT-reconstructed images (counts/voxel) were corrected for physical decay at each acquisition and measurement time point. CCF was calculated using the following equation:

$$CCF(SP)=planar\ counts/(SPECT\ counts\times V)$$

Study protocol

Table 1 summarizes the acquisition and SPECT reconstruction parameters. The masking on unsmoothed images method was consistently used in clinical practice. This method involves masking to extract the heart before smoothing during the reconstruction process to suppress the effects of subdiaphragmatic activity (23).

The acquisition flow is outlined as follows:

I. Rest acquisition

- A dose of ^{99m}Tc-MIBI (280 MBq) was administered. After placing ^{99m}Tc-MIBI in an extension tube, 15 mL of saline solution was injected intravenously at a constant rate of 1.5 mL/sec using an autoinjector.
- Dynamic anterior view images were acquired for 6 minutes, starting simultaneously with the intravenous injection.
- Blood pressure and heart rate measurements were recorded from the lower limbs at the start of the dynamic acquisition to calculate the rate pressure product (RPP).
- Myocardial perfusion-gated SPECT/CT was performed 45 minutes post-injection.
- The radioactivity of the syringe before and after administration was measured using a dose calibrator for analysis via the DOSE method.

II. EHL calculation

- Planar anterior view images were acquired for 1 minute, 45–60 minutes after the rest SPECT acquisition, to calculate the eHL.

III. Stress acquisition

- Adenosine (0.12 mg/min/kg) was continuously administered for 6 minutes. A dose of ^{99m}Tc-MIBI (660 MBq) was injected 3 minutes after the start of adenosine administration.
- The intravenous injection procedure was identical to that used during the rest acquisition.
- A 9-minute dynamic image acquisition was initiated 3 minutes before the intravenous injection to subtract residual counts from the dynamic images.
- Blood pressure and heart rate were recorded during ^{99m}Tc-MIBI administration in the lower limbs to calculate the RPP.
- Myocardial perfusion ECG-gated SPECT/CT was performed 45 minutes after the intravenous injection. The radioactivity measurement of the syringe followed the same procedure as during the rest phase.

Subject

Twenty-nine NV were selected based on criteria from the Japanese Society of Nuclear Medicine's normal database (24).

Twenty-two patients with IHD and stable disease (vascular stenosis rate ≧ 75%) who were scheduled for elective percutaneous coronary intervention were included. This group consisted of nine patients with single-vessel disease (SVD) and 13 patients with multivessel disease (MVD). Patients with a history of myocardial infarction were excluded.

Nine patients with nonischemic HF without significant coronary artery stenosis were retrospectively analyzed using

Table 2

Backgroud	NV	SVD	MVD	HF
Number	29	9	13	9
Age	55.4 ± 11.7	74.9 ± 8.8	71.5 ± 12.3	70.8 ± 8.9
Sex	M14/F15	M5/F4	M9/F4	M4/F5
Height (cm)	161.8 ± 9.8	160.2 ± 13.3	157.3 ± 11.2	152.8 ± 6.3*
Weight (kg)	61.4 ± 12.6	59.6 ± 16.2	61.2 ± 16.2	53.1 ± 9.8
BSA (m^2)	1.65 ± 0.20	1.62 ± 0.23	1.62 ± 0.27	1.48 ± 0.13*
BMI	23.2 ± 3.0	23.0 ± 1.8	24.8 ± 5.5	22.7 ± 0.39
Diabetes mellitus	4 (14%)	6 (67%)	5 (38%)	4 (44%)
Hypertension	7 (24%)	7 (78%)	12 (92%)	6 (67%)
Dyslipidemia	3 (10%)	6 (67%)	6 (46%)	0 (0%)
Smoking	3 (10%)	0 (0%)	6 (46%)	2 (22%)
CKD	0 (0%)	4 (44%)	3 (23%)	3 (33%)
Study conditions				
HR (/min) Stress	61.7 ± 6.9	64.4 ± 12.4	66.8 ± 15.8	70.9 ± 13.7*
Rest	73.0 ± 14.8####	65.7 ± 11.9	72.2 ± 19.2	79.8 ± 29.8
SBP (mmHg) Stress	149.6 ± 11.7	146.6 ± 29.2	158.9 ± 27.8	150.1 ± 28.9
Rest	146.4 ± 21.5	145.3 ± 37.2	154.3 ± 33.2	149.4 ± 24.5
DBP (mmHg) Stress	75.8 ± 10.0	65.3 ± 12.3*	76.9 ± 14.8	70.7 ± 9.4
Rest	74.2 ± 13.2	63.9 ± 11.8*	77.7 ± 15.1	72.3 ± 19.4
RPP Stress	9269 ± 1699	9461 ± 2623	10638 ± 3540	10594 ± 2476
Rest	10627 ± 2347###	9386 ± 2108	10911 ± 3231	12025 ± 4977

NV, normal volunteers; SVD, single-vessel disease; MVD, multivessel disease; HF, heart failure; BSA, body surface area (m2); BMI, body mass index (kg/m2); CKD, chronic kidney disease; HR, heart rate; SBP, systolic blood pressure; DBP, diastolic blood pressure; RPP, rate-pressure product.
P<0.0001 and ### P<0.001 (t-test between rest and stress), * P<0.05 (t-test with NV)

stress myocardial perfusion ECG-gated SPECT/CT. The resting ejection fraction (EF) was 40.8 ± 21.7, and both HF with reduced EF and HF with preserved EF were included.

The summed stress score for SVD was 0–3 in 1 case, 4–7 in 5 cases, and 8 or more in 3 cases; MVD was 0–3 in 6 cases, 4–7 in 3 cases, and 8 or more in 4 cases; and HF was 0–3 in 5 cases, 4–7 in 2 cases, and 8 or more in 2 cases.

Table 2 provides an overview of the background characteristics and study conditions of the NV, SVD, MVD, and HF groups.

This study was approved by the hospital's ethics committee. Informed consent was obtained from the NV group after the purpose, methods, and precautions of the study were explained using written documentation.

Study 1: Statistical analysis of each index

The normal ranges of the AUC-based and dose-based MFR indices were determined using the NV data. Additionally, we evaluated whether statistically significant differences existed between NV and SVD and between MVD and HF.

Study 2: Diagnostic accuracy of each index for SVD, MVD, and HF

The diagnostic accuracies of the AUC-based and dose-based MFR indices for SVD, MVD, and HF, in combination with NV, were assessed using ROC analysis.

Statistical analysis

All measurements were expressed as the mean ± standard deviation. Comparisons between measurements were performed using the Student's t-test. Differences were considered statistically significant at a risk level of $p<0.05$.

ROC analysis was used to determine significant differences between the AUCs, with DeLong's test applied for statistical comparison. Additionally, the cutoff values, sensitivity, and specificity were calculated using the Youden index.

Results

Study 1: Statistical analysis of each index

The results of this analysis are shown in Figure 1(A). The AUC-based MFR index was 1.63 ± 0.30 for NV, 1.40 ± 0.24 for SVD, 1.28 ± 0.17 for MVD, and 1.11 ± 0.12 for HF. In the t-test, significant differences were observed between MVD (P = 0.0004) and HF (P = 0.00002) compared with NV. No significant difference was observed between NV and SVD (P=0.052). Similarly, the dose-based MFR index was 1.18 ± 0.14 for NV, 1.15 ± 0.26 for SVD, 1.02 ± 0.10 for MVD, and

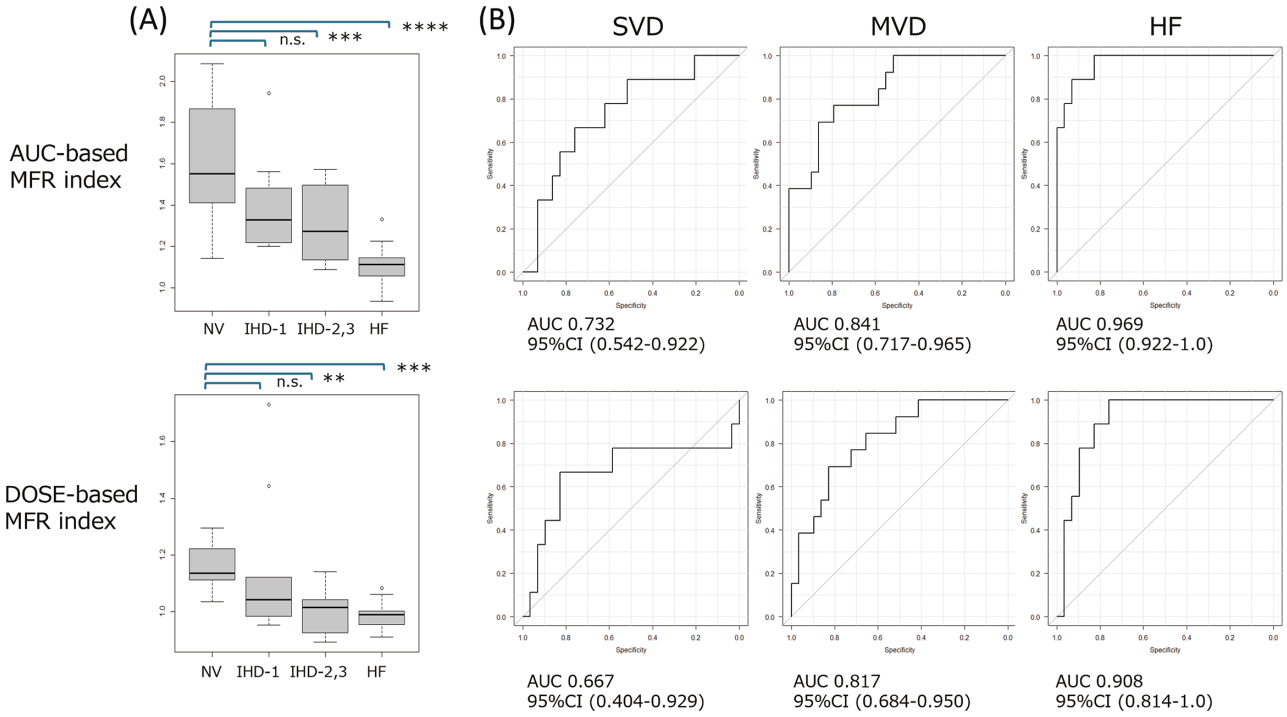

Figure 1 Analysis results of AUC-based MFR index and dose-based MFR index.
(A) Box-plot: Comparisons among NV, IHD-1, IHD-2&3 and HF.
AUC-based and dose-based MFR indices showed significant differences between NV and MDV or HF, but not between NV and SVD.
(B) ROC analysis of AUC-based MFR- and dose-based MFR indices.
The differences between the AUC-based MFR index and dose-based MFR indices were not significant.
NV, normal volunteers; SVD, single-vessel disease; MVD, multivessel disease; HF, heart failure; AUC, area under the ROC curve.
****:P<0.0001, ***:P<0.001, **:P<0.01, *:P<0.05 (t-test for NV).

0.99 ± 0.06 for HF. Significant differences were observed for the MVD (P=0.001) and HF (P=0.0005) groups compared with NV, while no significant difference was noted between NV and SVD (P=0.665).

Comparisons of the AUC-based MFR index and dose-based MFR index across NV, SVD, MVD, and HF groups revealed significant differences, with P<0.0001, P=0.019, P=0.0003, and P=0.037, respectively.

Diagnostic accuracy of each index in patients with SVD, MVD, and HF combined with NV

The results of the ROC analysis are shown in Figure 1(B). For the AUC-based MFR index, the AUC was 0.732 (95% CI: 0.542–0.922), with a sensitivity of 0.759 and a specificity of 0.667 at a cutoff value of 1.409 for SVD; 0.841 (95% CI: 0.717–0.965), with a sensitivity of 0.793 and a specificity of 0.769 at a cutoff value of 1.372 for MVD; and 0.969 (95% CI: 0.922–1.0), with a sensitivity of 0.828 and a specificity of 1.000 at a cutoff value of 1.322 for HF.

In contrast, for the dose-based MFR index, the AUC was 0.667 (95% CI: 0.404–0.929), with a sensitivity of 0.828 and a specificity of 0.667 at a cutoff value of 1.052 for SVD; 0.817 (95% CI: 0.684–0.950), with a sensitivity of 0.828 and a specificity of 0.692 at a cutoff value of 1.064 for MVD; and 0.908 (95% CI: 0.814–1.0), with a sensitivity of 0.759 and a specificity of 1.000 at a cutoff value of 1.082 for HF.

The AUC of the ROC analysis for the AUC-based and dose-based MFR indices in SVD, MVD, and HF showed no significant differences, as indicated by the DeLong's test (P=0.605, P=0.779, and P=0.281, respectively).

Typical examples are shown in Figure 2.

Discussion

Dynamic imaging during the administration of ^{99m}Tc-MIBI at rest and under stress is essential for obtaining the input function in the AUC method. However, this process reduces examination throughput, limiting its feasibility for routine clinical practice. If the MFR index could be accurately estimated from a standard SPECT MPI scan without requiring a dynamic scan, it would significantly enhance the practicality and adoption of these measurements in clinical settings.

Mekkaoui et al. reported that the clinical application of vasodilator stress for perfusion imaging requires careful consideration of the effects of vasodilating agents (adenosine or regadenosine) on systemic hemodynamics, coronary flow, radiotracer uptake, and clearance kinetics. The AUC method addresses these effects to some extent by incorporating the

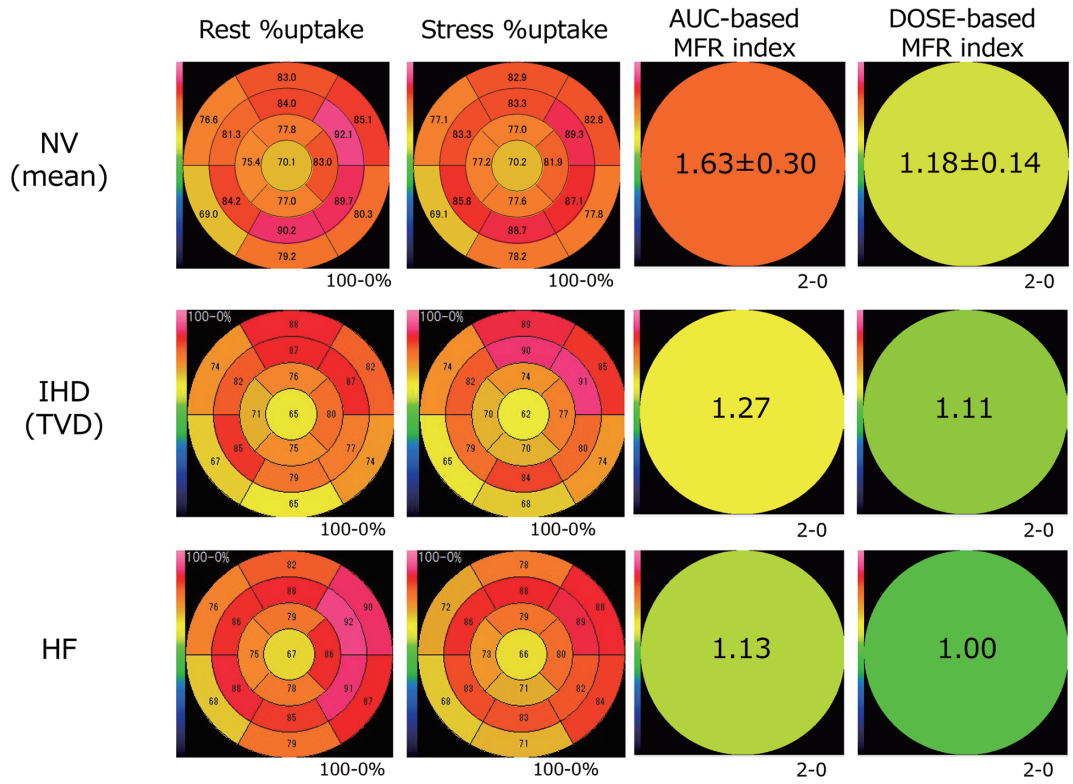

Figure 2　Typical examples.
Analysis results: AUC-based MFR index and dose-based MFR index in representative cases.
NV: normal volunteers, IHD: ischemic heart disease, HF: heart failure
Polar maps of NV (mean) and the two sample cases (IHD and HF).
IHD case: A 71year old patient with IHD and three-vessel disease (#2, 99%; #6, 75%; #11, 75%) presenting with exertional angina.
HF case: A 68 years old male with congestive heart failure secondary to mitral valve deviation syndrome and hypertension. No stenosis was identified in CAG.
The display conditions are 0-100% for the relative distribution (uptake) images and 0-2 for the MFR index images.

input function and the eHL of myocardial uptake in the analysis. In contrast, the DOSE method does not account for these variables, which may explain the significant differences observed between the AUC-based and dose-based MFR indices.

The accuracy of the DOSE method could potentially be improved by correcting for differences in cardiac function, such as heart rate (HR) and the heart RPP, between rest and stress conditions. However, in this study, there was a significant difference in HR and RPP between rest and stress in the NV group but not in the SVD, MVD, or HF groups, suggesting that cardiac function differences may have had minimal impact on the results.

No significant differences were observed between NV and SVD for either the AUC-based or dose-based MFR index. Additionally, the AUC of the ROC curve analysis for SVD tended to be lower than that for MVD and HF. In this study, the MFR index was used to evaluate the overall heart. As a result, it is possible that the MFR index was underestimated in one-vessel lesions due to the influence of normal regions. This limitation could potentially be addressed by incorporating regional analyses.

Although the quantitative analysis of ^{99m}Tc-MIBI is limited by its lower extraction rate and the roll-off phenomenon observed at higher myocardial blood flow, the results of this ROC analysis suggest that the AUC-based and dose-based MFR indices are clinically applicable.

Conclusion

The clinical application of the AUC and DOSE methods for MFR index quantitative analysis using an Anger-type SPECT/CT system has the potential to improve diagnostic and prognostic accuracy in patients with IHD and HF.

Acknowledgments

None.

Sources of funding

None.

Conflicts of interest

The authors declare no conflicts of interest related to this study.

Reprint requests and correspondence:
Atsushi Komuro
Department of Radiology, Shirakawa Kosei General Hospital, Toyochikamiyajiro 2-1, Shirakawa City, Fukushima, 961-0005 Japan
E-mail: komuro_a@kvj.biglobe.ne.jp

References

1. Berman DS, Kang X, Slomka PJ, et al. Underestimation of extent of ischemia by gated SPECT myocardial perfusion imaging in patients with left main coronary artery disease. J Nucl Cardiol 2007; 14: 521–8.
2. Reyes E. Detection of left main stem and three-vessel coronary artery disease by myocardial perfusion SPECT imaging. EuroIntervention 2010; 6 Suppl G: G72–8.
3. Lopes NH, da Silva Paulitsch F, Gois AF, et al. Impact of number of vessels disease on outcome of patients with stable coronary artery disease: 5-year follow-up of the Medical, Angioplasty, and bypass Surgery Study (MASS). Eur J Cardiothorac Surg 2008; 33: 349–54.
4. Jones EL, King SB 3rd, Craver JM, et al. The spectrum of left main coronary artery disease: Variables affecting patient selection, management, and death. J Thorac Cardiovasc Surg 1980; 79: 109–16.
5. Slomka P, Berman DS, Germano G. Myocardial blood flow from SPECT. J Nucl Cardiol 2017; 24: 278–81.
6. Murthy VL, Naya M, Foster CR, et al. Improved cardiac risk assessment with noninvasive measures of coronary flow reserve. Circulation 2011; 124: 2215–24.
7. Ziadi MC, Dekemp RA, Williams KA, et al. Impaired myocardial flow reserve on rubidium-82 positron emission tomography imaging predicts adverse outcomes in patients assessed for myocardial ischemia. J Am Coll Cardiol 2011; 58: 740–8.
8. Ziadi MC, Dekemp RA, Williams K, et al. Does quantification of myocardial flow reserve using rubidium-82 positron emission tomography facilitate detection of multivessel coronary artery disease? J Nucl Cardiol 2012; 19: 670–80.
9. Naya M, Murthy VL, Taqueti VR, et al. Preserved coronary flow reserve effectively excludes high-risk coronary artery disease on angiography. J Nucl Med 2014; 55: 248–55.
10. Bober RM, Milani RV, Oktay AA, et al. The impact of revascularization on myocardial blood flow as assessed by positron emission tomography. Eur J Nucl Med Mol Imaging 2019; 46: 1226–39.
11. Slart RHJA, Zeebregts CJ, Hillege HL, et al. Myocardial perfusion reserve after a PET-driven revascularization procedure: A strong prognostic factor. J Nucl Med 2011; 52: 873–9.
12. Wells RG, Timmins R, Klein R, et al: Dynamic SPECT measurement of absolute myocardial blood flow in a porcine model. J Nucl Med 2014; 55: 1685–91.
13. Ben-Haim S, Murthy VL, Breault C, el al. Quantification of myocardial perfusion reserve using dynamic SPECT imaging in humans: A feasibility study. J Nucl Med 2013; 54: 873–9.
14. Tsukamoto T, Ito Y, Noriyasu K, et al. Quantitative assessment of regional myocardial flow reserve using tc-99m-sestamibi imaging--Comparison with results of O-15 water PET. Circ J 2005; 69: 188–93.
15. Nose N, Fukushima K, Lapa C, et al. Assessment of coronary flow reserve using a combination of planar first-pass angiography and myocardial SPECT: Comparison with myocardial ^{15}O-water PET. Int J Cardiol 2016; 222: 209–12.
16. Taki J, Fujino S, Nakajima K, et al. ^{99m}Tc-sestamibi retention characteristics during pharmacologic hyperemia in human myocardium: Comparison with coronary flow reserve measured by Doppler flowire. J Nucl Med 2001; 42: 1457–63.
17. Sugihara H, Yonekura Y, Kataoka K, Fukai D, Kitamura N, Taniguchi Y. Estimation of coronary flow reserve with the use of dynamic planar and SPECT images of Tc-99m tetrofosmin. J Nucl Cardiol 2001; 8: 575–9.
18. Ito Y, Katoh C, Noriyasu K, et al. Estimation of myocardial blood flow and myocardial flow reserve by ^{99m}Tc-sestamibi imaging: Comparison with the results of [^{15}O]H_2O PET. Eur J Nucl Med Mol Imaging 2003; 30: 281–7.
19. Storto G, Cirillo P, Vicario MLE, et al. Estimation of coronary flow reserve by Tc-99m sestamibi imaging in patients with coronary artery disease: Comparison with the results of intracoronary Doppler technique. J Nucl Cardiol 2004; 11: 682–8.
20. Fujiwara S, Takeishi Y, Atsumi H, Chiba J, Takahashi K, Tomoike H. Quantitative assessment of myocardial ^{99m}Tc-sestamibi uptake during exercise: Usefulness of response rate for assessing severity of coronary artery disease. Jpn Circ J 1998; 62: 592–8.
21. Komuro A, Teraoka S, Hosoya T, et al. Development of a new uptake ratio measurement method for myocardial blood flow quantitative evaluation in myocardial perfusion SPECT. Jpn J Nucl Med Technol 2015; 35: 199–207. [In Japanese]
22. Kanda Y, Investigation of the freely available easy-to-use software 'EZR' for medical statistics. Bone Marrow Transplant 2013; 48: 452–8.
23. Komuro A, Teraoka S, Ishikawa Y, et al. A novel method to suppress the effect of subdiaphragmatic activity in ^{99m}Tc myocardial perfusion SPECT and evaluation of its usefulness using a myocardial phantom. Ann Nucl Cardiol 2022; 8: 30–5.
24. Nakajima K, Kumita S, Ishida Y, et al. Creation and characterization of Japanese standards for myocardial perfusion SPECT: Database from the Japanese Society of Nuclear Medicine Working Group. Ann Nucl Med 2007; 21: 505–11.
25. Mekkaoui C, Jadbabaie F, Dione DP, et al. Effects of adenosine and a selective A2A adenosine receptor agonist on hemodynamic and thallium-201 and technetium-99m-sestaMIBI biodistribution and kinetics. JACC Cardiovasc Imaging 2009; 2: 1198–208.
26. Zaret BL, Beller GA. Clinical nuclear cardiology: State of the art and future directions. 3rd ed. Elsevier Mosby, Philadelphia, PA, 2005: 216.